ACS APPLIED MATERIALS & INTERFACES

Research Article

www.acsami.org

Dual-Microstructured Porous, Anisotropic Film for Biomimicking of Endothelial Basement Membrane

Zuyong Wang,[†] Swee Hin Teoh,[‡] Minghui Hong,[§] Fangfang Luo,[§] Erin Yiling Teo,[⊥] Jerry Kok Yen Chan,*[,⊥,∥,⊗] and Eng San Thian*[,†]

[†]Department of Mechanical Engineering, National University of Singapore, 9 Engineering Drive 1, Singapore 117576, Singapore

[‡]School of Chemical and Biomedical Engineering, Nanyang Technological University, Singapore 637459, Singapore

[§]Department of Electrical and Computer Engineering, National University of Singapore, 2 Engineering Drive 3, Singapore 117576, Singapore

[⊥]Department of Reproductive Medicine, KK Women's and Children's Hospital, 100 Buikit Timah Road, Singapore 229899, Singapore

[∥]Department of Obstetrics and Gynaecology, Yong Loo Lin School of Medicine, National University of Singapore, 14 Medical Drive, Singapore 117599, Singapore

[⊗]Cancer and Stem Cell Biology, Duke-NUS Graduate Medical School, 8 College Road, Singapore 169857, Singapore

ABSTRACT: Human endothelial basement membrane (BM) plays a pivotal role in vascular development and homeostasis. Here, a bioresponsive film with dual-microstructured geometries was engineered to mimic the structural roles of the endothelial BM in developing vessels, for vascular tissue engineering (TE) application. Flexible poly(ε-caprolactone) (PCL) thin film was fabricated with microscale anisotropic ridges/grooves and through-holes using a combination of uniaxial thermal stretching and direct laser perforation, respectively. Through optimizing the interhole distance, human mesenchymal stem cells (MSCs) cultured on the PCL film's ridges/grooves obtained an intact cell alignment efficiency. With prolonged culturing for 8 days, these cells formed aligned cell multilayers as found in native tunica media. By coculturing human umbilical vein endothelial cells (HUVECs) on the opposite side of the film, HUVECs were observed to build up transmural interdigitation cell−cell contact with MSCs via the through-holes, leading to a rapid endothelialization on the PCL film surface. Furthermore, vascular tissue construction based on the PCL film showed enhanced bioactivity with an elevated total nitric oxide level as compared to single MSCs or HUVECs culturing and indirect MSCs/HUVECs coculturing systems. These results suggested that the dual-microstructured porous and anisotropic film could simulate the structural roles of endothelial BM for vascular reconstruction, with aligned stromal cell multilayers, rapid endothelialization, and direct cell−cell interaction between the engineered stromal and endothelial components. This study has implications of recapitulating endothelial BM architecture for the *de novo* design of vascular TE scaffolds.

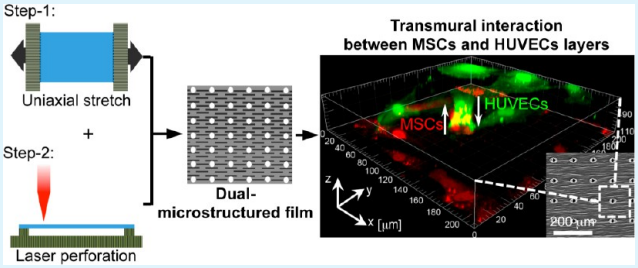

KEYWORDS: *endothelial basement membrane, porous micropatterned film, cellular alignment, cell−cell interaction, vascular tissue engineering*

INTRODUCTION

Current therapeutic approaches for cardiovascular diseases, the global leading cause of death, remain inadequate for many patients.[1] Tissue engineering (TE) offers a promising route for the improvement or regeneration of diseased vessel function using a combination of biomaterials, cells and engineering techniques.[2] However, vascular TE grafts presently have limitations in the mechanical (e.g., unmatched compliance)[3] and biological (e.g., prothrombotic nature)[4] functions to hinder their clinical translation. To construct proper vascular TE grafts, tissue engineers have been looking for the recapitulation of developmental elements, which establish natural vessel structure and physiological function. The endothelial basement membrane (BM) located between tunica media and intima is such a key targeted evolutionary component, and acts a pivotal role as the basolateral of stromal and endothelial cells, for both vascular development[5] and maintenance of the adult vessel function.[6]

Human endothelial BM is composed of a three-dimensional (3D) architecture with highly porous and organized laminin/collage IV networks.[6,7] The importance of such architecture for designing vascular TE grafts has been revealed by how substrates biomimicking endothelial BM such as the roughness,[8] anisotropy[9,10] and porosity[11] can influence enhanced cell

Received: March 20, 2015
Accepted: June 1, 2015
Published: June 1, 2015

DOI: 10.1021/acsami.5b02464
ACS Appl. Mater. Interfaces 2015, 7, 13445−13456

adhesion, spreading, proliferation and specific gene expressions in smooth muscle cells (SMCs) and endothelial cells (ECs). Such architectural simulation on TiO substrate has also been shown to impact ECs mobility and differentiation over surface chemistry.[12] However, these substrates are designed with singular structure, and cannot mimic the architectural complexity of endothelial BM such as coexistence of the anisotropy[7] and holes.[13−16] For example, the endothelial BM of developing vessel is not entirely continuous, and has gaps to allow direct interaction between the ECs and perivascular stromal cells such as pericytes[14,15] and SMCs,[13,16,17] importantly for preventing nascent vessel regression. Furthermore, the 3D architecture of endothelial BM guides both SMCs and ECs with specific localization, to form the unique vessel structure and function such as the aligned SMCs multilayers in tunica media for mechanical strength and compliance support.[2,3]

The current engineered solutions of endothelial BM have not addressed simulation of the architectural complexity. Here, we report a flexible dual-microstructured thin film to mimic the structural roles of the endothelial BM in developing vessels, for promoting vascular reconstruction. This bioresponsive film will be able to facilitate vascular reconstruction through guiding stromal cells to form aligned cellular multilayers on the film's tunica media surface, while promoting endothelialization on the film's tunica intima side via direct transmural cell−cell interaction.

EXPERIMENTAL SECTION

Materials. Poly(ε-caprolactone) (PCL, M_W = 80 000), phosphate buffer saline (PBS), penicillin−streptomycin (PS), TRITC-conjugated phalloidin, paraformaldehyde (PFA), triton-X 100, bovine serum albumin (BSA), 4′,6-diamidino-2-phenylindole (DAPI) and PHK cell linker dye kits were purchased from Sigma-Aldrich (Singapore). Fetal bovine serum (FBS), Trypsin−EDTA and Dulbecco's modified Eagle medium (DMEM) were purchased from Life Technologies (Singapore), endothelial cell growth medium (EGM) from Lonza (Singapore), and NO assay kits from Cell Biolabs, Inc. (USA). Tissue culture plates (TCP) and flasks, and low-adhesion cell culture plates were purchased from Thermo Fisher Scientific (USA), Nunc (Singapore), and Corning (Costar, Singapore), respectively.

Preparation of Dual-Microstructured PCL Films. Flexible PCL thin films were engineered with dual-microstructured geometries through a combination of uniaxial thermal stretching and direct femtosecond laser perforation (Figure 1). PCL solid mass after two-roll milling was heat pressed at 80 °C and 300 MPa into a thick film named HP-PCL. The film was then subjected to uniaxial stretching at 54 °C with a draw ratio of 4. The uniaxial-stretched PCL film was thinner and named as UX_{HP}-PCL. To perforate the PCL films, a Ti:sapphire femtosecond laser was used with a wavelength of 800 nm, pulse duration of 110 fs and repetition rate of 1 kHz (Spectra-Physics, USA). Laser beam scanning was controlled using a U500 MMI software (Aerotech, UK). HP-PCL and UX_{HP}-PCL after femtosecond laser perforation were named as PHP-PCL and PUX_{HP}-PCL, respectively.

Morphological Characterization of PCL Films. PCL film samples were sputter-gold coated at 10 mA for 30 s, and imaged using field emission scanning electron microscopy (SEM; S-4300, Hitachi, Japan) at different magnifications with an accelerating voltage of 15 kV.

Cell Isolation and *in Vitro* Culture. Human tissue collection for research purposes was approved by the Domain Specific Review Board of National Healthcare Group, in compliance with international guidelines regarding to the use of fetal tissues for research.[18] In all cases, patients gave separate written consent for the use of their collected tissues.

Mesenchymal stem cells (MSCs) were isolated from human fetal bone marrow as previously described.[2] Single-cell suspension from the

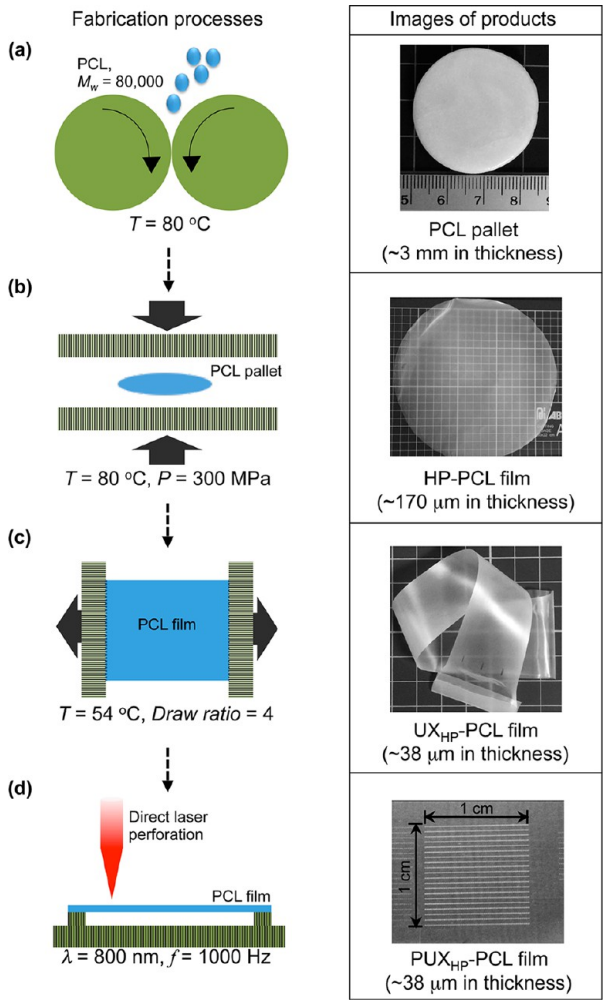

Figure 1. Schematic diagrams illustrating the fabrication of flexible dual-microstructured thin film. (a) Two-roll milling. (b) Heat pressing. (c) Uniaxial stretching. (d) Direct laser perforation.

marrow components of femurs was seeded in a tissue culture flask at a density of 10^6 cells/cm^2. Nonadherent cells were removed after 3 days of culturing in D10 medium (DMEM + 10% FBS + 1% PS). The adherent cells were further cultured for 1 week, recovered and characterized with stem cell phenotype.[2] GFP-labeled human umbilical vein endothelial cells (HUVECs) were derived as previously reported,[19] and provided by Mr. Sandikin Dedy (National University of Singapore, Singapore).

Cell Morphology and Organization. Cell morphology was characterized through a fixed-cell cytoskeletonal staining as previously described.[20] MSCs (5000 cells/cm^2) were seeded on UX_{HP}-PCL (control group) and PUX_{HP}-PCL, and cultured in D10 medium for 3 days. After PBS washing, the cells were fixed and permeabilized by PFA (3.7% in PBS; for 15 min) and Triton-X 100 (0.1% in PBS; for 5 min), respectively. Cells were then washed with PBS thrice, blocked by BSA (2% in PBS; for 30 min) and incubated with TRITC-conjugated phalloidin (1:200 in PBS; for 60 min) for F-actin labeling. After PBS washing thrice, the cells were further incubated with DAPI (1:1000 in PBS; for 5 min) for nucleus DNA labeling. Cells were imaged using a confocal laser scanning microscopy (CLSM; (FV1000, Olympus, Japan) under identified parameters for all samples.

Cell organization was characterized through a live-cell cytoplasmic staining as previously described.[2,18] MSCs were seeded on PCL films and cultured in D10 medium for predetermined periods. HP-PCL and UX_{HP}-PCL were used as negative and positive control, respectively. After PBS washing thrice, the cells were fluoresence-labeled using FDA (5 μg/L; for 10 min) at room temperature. Cells after further PBS

DOI: 10.1021/acsami.5b02464
ACS Appl. Mater. Interfaces 2015, 7, 13445−13456

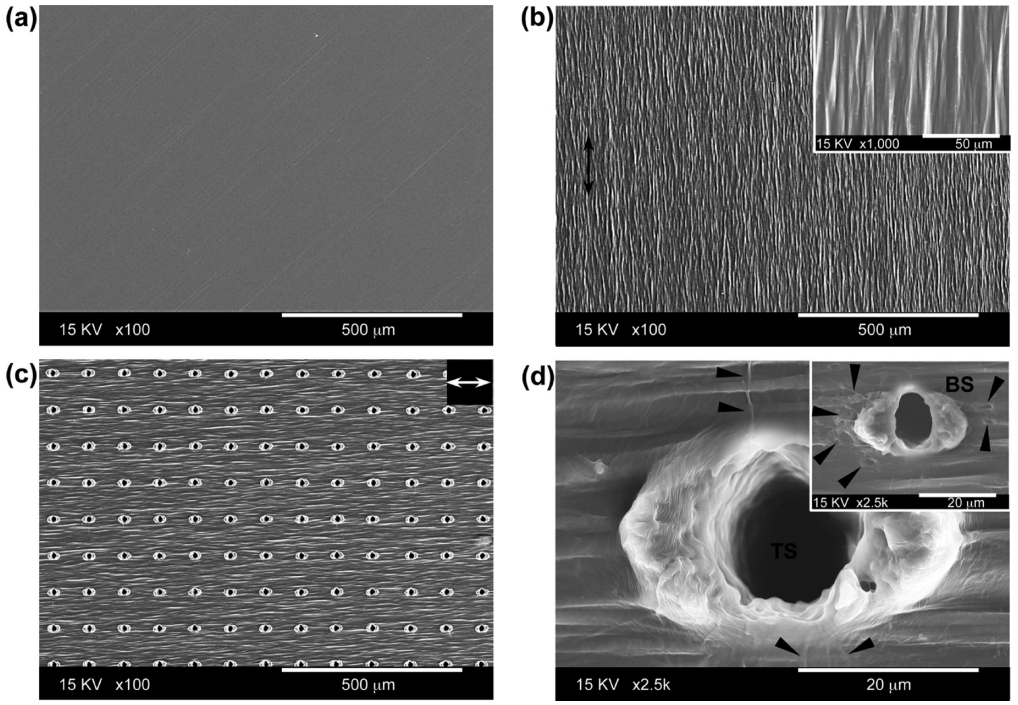

Figure 2. Scanning electron microscopy (SEM) images of PCL films. (a) Flat topography of HP-PCL. (b) Anisotropic topography of UX_{HP}-PCL composed of orientated microscale ridges and grooves (inset: high-magnified SEM image; double-headed dark arrow, stretching direction). (c,d) Dual-microstructured topography of PUX_{HP}-PCL with orientated ridges/grooves and through-holes (TS, film top surface; BS, film bottom surface; inset: SEM image of BS; double-headed white arrow, stretching direction; dark arrow, melting ejecta-induced surface damages).

washing were immediately imaged using CLSM under a low powered magnification of ×10. Image analysis was performed using the built-in function of NIH ImageJ software (USA), with fluorescence from the hole scattering and the cells that were in contact with other cells and image edges being manually removed from the data sets.[18] Cellular angle was determined as an orientation of the major elliptic axis of individual cell. A preferential cell orientation has been determined and set as 0°. All cellular angles were then normalized to the preferential cell orientation. The number of cells within each degree from −90° to +89° was calculated and normalized such that the total sum was unity. Cells with angles falling into ±10° was considered to be aligned.[18] For comparison, the cell alignment efficiency of each group was finally normalized to that of positive control, which has a value of 1. Three film samples were used for each experimental group.

Direct Cell−Cell Interaction. Fluorescence labeling was performed for different cells for the visualization of direct cell−cell interaction across PUX_{HP}-PCL. MSCs were labeled with red fluorescence using a PHK-26 kit. Cells collected from culture expanding were resuspended in Diluent (2× final concentration, 0.5 mL). PHK26 dye was diluted into a 2× solution (0.5 mL). The cell suspension and PHK26 dilution were then mixed, and incubated at 21 °C for 5 min. Fluorescence-labeling reaction was stopped by adding 1 mL FBS. Lenti-virally infected GFP HUVECs was identified with green fluorescence.

An in-house designed ring was used for coculturing MSCs and HUVECs on the two surfaces of PUX_{HP}-PCL, respectively. PHK26-labeled MSCs (10 000 cells/cm^2) were first seeded on PUX_{HP}-PCL for 1 day of culturing in D10 medium. The film was then flipped over to transfer to the ring. GFP-labeled HUVECs (20 000 cells/cm^2) were seeded on the film opposite side of MSCs. MSCs/HUVECs coculturing was performed in EGM10 medium, which has been shown to support the growth and maintenance of MSCs and HUVECs. The cells after 3 days of coculturing were imaged with CLSM using a z-scanning model. Images were reconstructed using the built-in function of Imaris software (Bitplane, Switzerland). The PHK26-labeled MSCs and GFP-labeled HUVECs were identified with red and green fluorescences, respectively. The MSCs−HUVECs contact was characterized as the colocalization of the red and green colors, represented as yellow color.

Cell Adhesion and Proliferation. To investigate endothelialization on PUX_{HP}-PCL, the cell number of HUVECs was assessed by enumerating nucleus number as previously reported.[21] GFP-labeled HUVECs, after seeding on the film opposite side of MSCs, were cocultured for 24 h to allow fully cellular adhesion, and cocultured for another 4 days for proliferation. Cells were then fixed, permeabilized and blocked. Cells were then incubated with DAPI (1:1000 in PBS; for 5 min) for cell nucleus labeling. The nucleus number of HUVECs was counted using the built-in function of NIH ImageJ software, with cells that have either green- or blue-fluorescence alone being manually removed from the data sets. Cell nucleus number enumerated at day 1 and 5 represented the adhesion and proliferation of HUVECs on the PCL film surface, respectively. Single-culture of HUVECs alone on UX_{HP}-PCL and PUX_{HP}-PCL, and coculture of HUVECs and MSCs on UX_{HP}-PCL via indirect cell−cell interaction were also investigated as comparison groups. Three samples were used for each experimental group.

Total NO Level. To evaluate the bioactivity of the vascular tissue construct, the system total NO level was investigated using a NO assay kit. MSCs and HUVECs were seeded on PCL films, and cultured in EGM10 medium in 12-well TCP (2.5 mL/well) for 8 days. At day 3 and 5, 0.5 mL of new EGM10 medium was added for nutrition supplement. Experimental groups of (G1) EGM10 medium alone, (G2) MSCs cultured on PUX_{HP}-PCL in EGM10 medium, (G3) HUVECs cultured on PUX_{HP}-PCL in EGM10 medium, (G4) coculturing of HUVECs/MSCs using UX_{HP}-PCL in EGM10 medium and (G5) coculturing of HUVECs/MSCs using PUX_{HP}-PCL in EGM10 medium were investigated. The total nitrate/nitrite (NO_3^-/NO_2^-) level in culture medium was examined following the procedures of NO assay kit. Briefly, cell culture medium (10 μL) was added to a 96-well plate and adjusted to 80 μL using assay buffer. 10 μL of enzyme cofactors and 10 μL of nitrate reducer were added in sequence, and incubated at 21 °C for 30 min for reducing nitrate into nitrite. After 2,3-diaminonaphthalene (10 μL) was added followed by incubation for 10 min, NaOH solution (20 μL) was added to stop the

DOI: 10.1021/acsami.5b02464
ACS Appl. Mater. Interfaces 2015, 7, 13445−13456

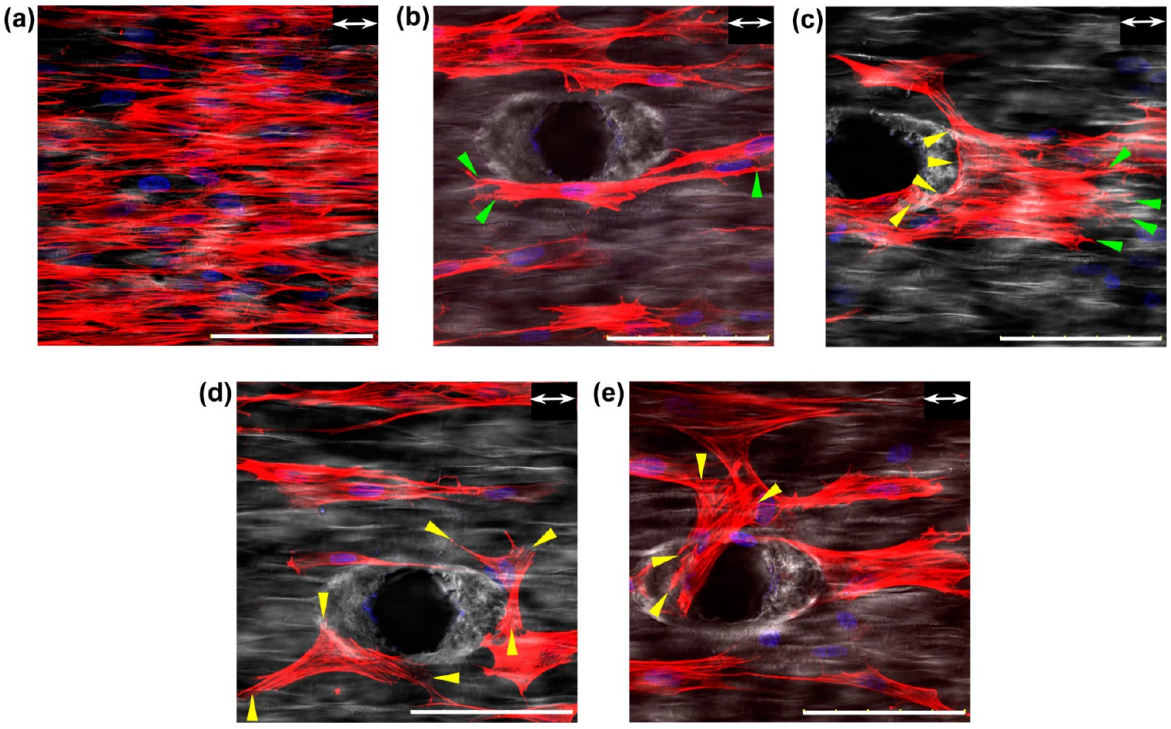

Figure 3. Confocal laser scanning microscopy (CLSM) images of MSCs. Human MSCs (5000 cells/cm^2) were cultured on UX_{HP}-PCL (positive control: Pos Ctrl) and PUX_{HP}-PCL for 3 days, and labeled with cytoskeleton F-actin (phalloidin: red color) and nucleus DNA (DAPI: blue color). (a) Aligned cell organization of MSCs along the ridges/grooves for Pos Ctrl (scale bar = 100 μm). (b–e) Cell organizational responses of MSCs to the dual-microstructured topography of PUX_{HP}-PCL as (b) retained cell alignment, (c) half-cell alignment, or aberrant cell organization to (d) cross over the ridges/grooves or (e) bridge the hole opening (double-headed white arrow, ridge direction; green arrow, free cell extension; yellow arrow, cell extension being obstructed or crossing to attach to the adjacent film surface points; scale bar = 100 μm).

reaction with enhanced fluorescence intensity. To prepare the standard curve, 10 μL EGM10 medium with 70 μL assay buffer was used as the blank, and 10 μL EGM10 medium with 20 μL assay buffer and 50 μL nitrate standards (0.156 to 10 μmol/L) was used as gradient. Fluorescence intensity was detected using a microplate reader at an excitation wavelength of 360 nm and emission wavelength of 430 nm. Basal fluorescence intensity of EGM10 medium was deducted from all groups. Three samples were used for each experimental group.

Statistical Analysis. Data analysis was performed on Prism 5 software. Results were reported as mean ± SD. A value of $p < 0.05$ was considered to be statistically significant.

RESULTS AND DISCUSSION

Characterization of Dual-Microstructured PCL Film. PCL was selected to fabricate the dual-microstructured film because of its unique properties of bioresorbability, competent mechanical strength, long-term fatigue resistance and low cost for vascular TE application.[2,22] Figure 1 shows the schematic diagrams for PCL film fabrication. The fabricated film of HP-PCL was thick (~170 μm), and after thermally uniaxial stretching, it became flexible and thinner (UX_{HP}-PCL: ~38 μm). SEM images show that HP-PCL possessed a flat film surface (Figure 2a), whereas UX_{HP}-PCL exhibited an anisotropic 3D topography composed of microscale ridges and grooves (ridge-length, ~90 μm; inter-ridge distance, ~6 μm; ridge-depth: 200–900 nm; Figure 2b). During uniaxial stretching, these ridges and grooves resulted in consistent orientations aligned along the stretching direction. The recrystallized PCL crystal and amorphous structures were postulated to form the ridges and grooves, respectively.[18]

Noncontact femtosecond laser engineering was then used to incorporate through-holes on the dense film of UX_{HP}-PCL (Figure 1d). This laser technique is now highly valuable for the use in tissue-engineering scaffold's processing such as surface patterning and 3D fabrication using two-photon polymerization,[23] and here, we showed scalable laser perforation in a large surface area of the flexible PCL thin film (e.g., 1 × 1 cm). Figure 2c demonstrates SEM images of the laser-perforated film of PUX_{HP}-PCL at a pulse energy of 20 μJ and pulse number of 60. Laser ablation resulted in *in situ* holes at the positions where laser–material interaction occurred. Because of the short laser–material interaction time of femtoseconds,[24] this laser ablation did not cause burrs or heat-affected zones on the PCL film. The hole pattern obtained was at a controllable interhole distance, without the use of templates or solvents for structural development. Figure 2d shows SEM images of the film top and bottom surfaces of PUX_{HP}-PCL. The hole exhibited a through-tunnel (~10 μm in diameter), with a pair of labial melting structures and fibrous redeposition of the sputtering PCL melt. This incorporation of through-holes to micropatterned biofilms has not been reported previously. The femtosecond laser-induced material's removal was attributed to both the photochemical and photothermal effects.[25]

Previously, electrospinning has been of great interest in generating analogous nano/microscale fibers to simulate endothelial BM architecture.[26,27] However, to obtain the structural anisotropy, uniaxial pulling was typically required during fibrogenesis, resulting in significant fiber packing with reduced porosity to restrict cell ingrowth.[28] Although chemical etching,[29] lithography[30] and soft lithography[10,31] have also been investigated to fabricate bioinspired substrates, they were still restricted by the intricate procedures, and limited in the development of appropriate masters for realizing complex

DOI: 10.1021/acsami.5b02464
ACS Appl. Mater. Interfaces 2015, 7, 13445–13456

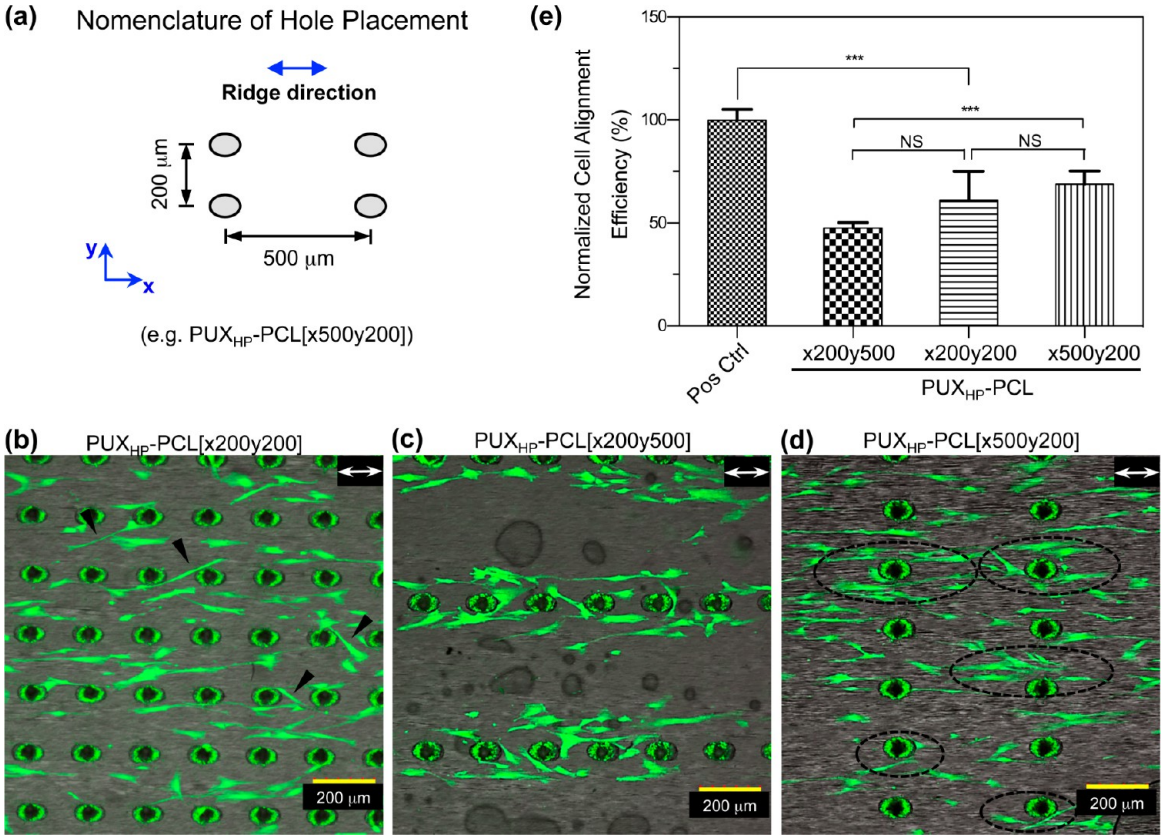

Figure 4. Cell alignment efficiencies of PUX$_{HP}$-PCL with different spatial hole distributions. MSCs (5000 cells/cm^2) after culturing on UX$_{HP}$-PCL (positive control: Pos Ctrl) and PUX$_{HP}$-PCL for 3 days were labeled using live-cell cytoplasmic staining (FDA: green color). (a) Schematic diagram illustrating the nomenclature of hole placement for PUX$_{HP}$-PCL. (b–d) CLSM images and (e) quantitative analysis of cell alignment efficiencies for MSCs cultured on PUX$_{HP}$-PCL[x200y200], PUX$_{HP}$-PCL[x200y500] and PUX$_{HP}$-PCL[x500y200] showed the influences of hole placement on MSCs organization (double-headed white arrow, ridge direction; dark arrow, aberrant cell extension between the holes in *x*-axis; dark circle, cells approaching the holes; $n = 3$; ***, $p < 0.001$; NS, $p > 0.05$).

structural features on flexible thin films. Furthermore, these methods involved drawbacks such as the unstable large-scale yield and chemical solvent usage and residual remains.[18] In contrast, this study developed a combined two-step method of uniaxial stretching and direct laser perforation, to engineer dual-microstructured ridges/grooves and through-holes on flexible PCL thin film. The fabrication was in large-scale, reproducible and solvent-free. Such as-fabricated PCL film could recapitulate the structural characteristics of the endothelial BM in developing vessels such as the anisotropy[7] and intermittent holes.[13−17]

Aligned Stromal Cell Organization on PUX$_{HP}$-PCL Surface. PUX$_{HP}$-PCL was used to reconstruct the aligned cell organization as in tunica media components of blood vessels. Figure 3a–e shows CLSM images of MSCs stained with F-actin/DNA. The cells cultured on UX$_{HP}$-PCL exhibited an aligned organization, with orientated cytoskeleton stress filaments along the ridges (Figure 3a). However, with the presence of laser-induced holes, MSCs alignment behavior varied according to the hole edges in different responses. As shown in Figure 3b, MSCs retained the cell alignment along ridges/grooves, where the cells were able to extend freely. In contrast, when MSCs encountered a hole along their axes, the cells wrapped around the circumference of the labial melt, whereas the other half of the cells remained aligned along the ridges/grooves on the film (Figure 3c). In some instances, MSCs organization has also been observed to deviate from the orientation of the ridges (Figure 3d), and in others, partial bridging of the hole opening has been found (Figure 3e). These observations showed various cell organizational responses to the combinatory presence of dual-microstructured ridges/grooves and through-holes of PUX$_{HP}$-PCL.

To investigate the influences of laser-induced holes on the cell alignment efficiency elicited by ridges/grooves, MSCs were cultured on PUX$_{HP}$-PCL with different spatial hole distribution. Figure 4a shows the nomenclature of hole placement, with *x*- and *y*-axes representing the parallel and perpendicular directions to the ridges, respectively. Figure 4b–d shows CLSM images of live-cell cytoplasmic staining of MSCs. On PUX$_{HP}$-PCL[x200y200], MSCs aligned only along parts of the film with continuous undisrupted ridges/grooves, whereas the cells growing between holes in *x*-axis tended to extend away from the ridge direction (Figure 4b). Comparatively, on PUX$_{HP}$-PCL[x200y500], there was crowding of the cells around the holes in the ridge direction (Figure 4c). However, MSCs cultured on PUX$_{HP}$-PCL[x500y200] extended more freely to align between holes in the direction of *x*-axis, with some approaching the holes (Figure 4d).

Quantitative analysis of cell angles showed that compared to Pos Ctrl of the UX$_{HP}$-PCL group, the presence of laser-induced holes resulted in declined alignment efficiencies for MSCs cultured on all three different PUX$_{HP}$-PCL (47.5–68.8% of Pos Ctrl, $p < 0.001$; Figure 4e). Compared to PUX$_{HP}$-PCL-[x200y200], MSCs cultured on PUX$_{HP}$-PCL[x200y500]

DOI: 10.1021/acsami.5b02464
ACS Appl. Mater. Interfaces 2015, 7, 13445−13456

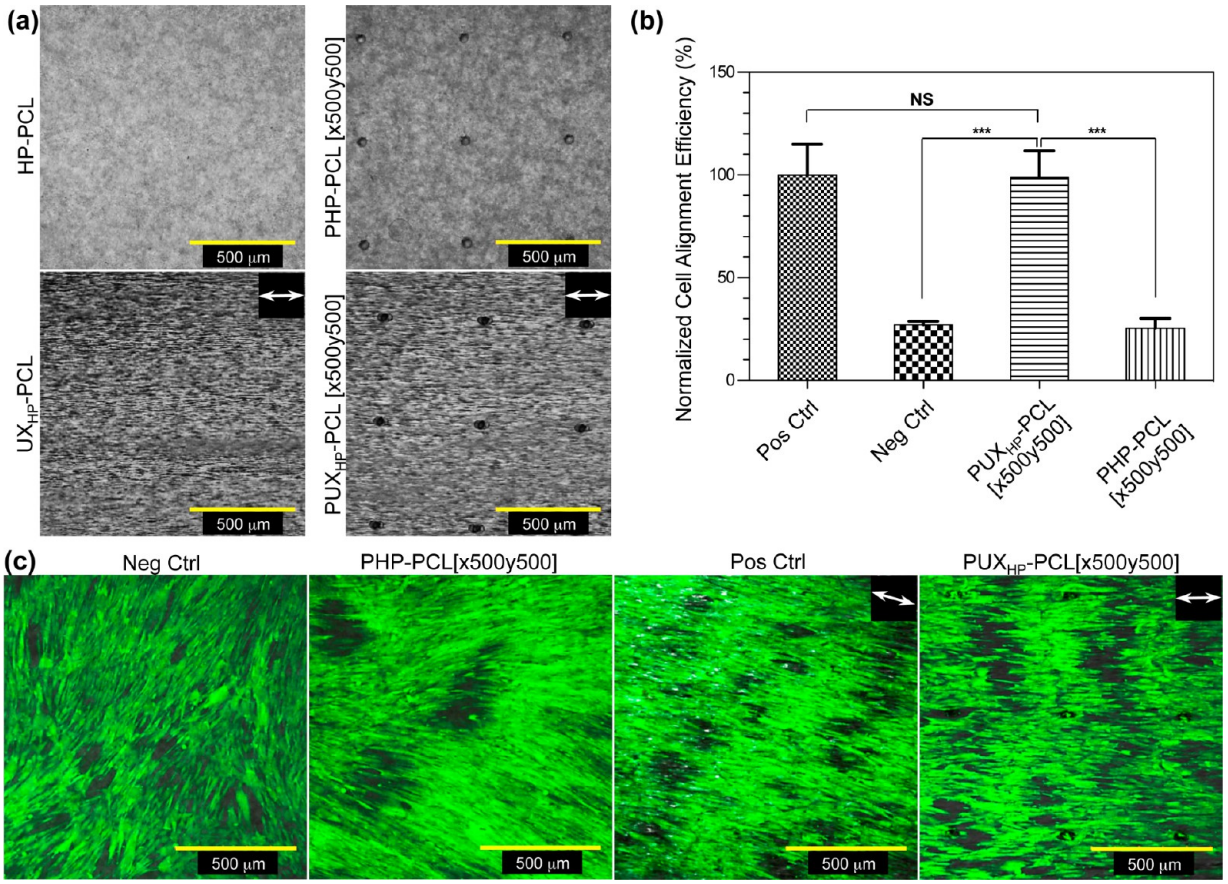

Figure 5. PUX$_{HP}$-PCL[x500y500] resulted in aligned cell multilayers. MSCs (5000 cells/cm^2) were seeded on HP-PCL (negative control: Neg Ctrl), PHP-PCL[x500y500], UX$_{HP}$-PCL (positive control: Pos Ctrl) and PUX$_{HP}$-PCL[x500y500] for 3 and 8 days of culturing, and labeled using live-cell cytoplasmic staining (FDA: green color). (a) CLSM DIC images of various PCL films. (b) Cell alignment efficiencies of MSCs after 3 days of culturing. MSCs on PUX$_{HP}$-PCL[x500y500] exhibited a comparable cell alignment efficiency to that of Pos Ctrl (n = 3; ***, p < 0.001; NS, p > 0.05). (c) CLSM images of MSCs after 8 days of culturing. MSCs reached confluence, and formed the aligned cell multilayers on PUX$_{HP}$-PCL[x500y500] as in Pos Ctrl (double-headed white arrow, ridge direction).

showed lower cell alignment efficiency ([x200y500] vs [x200y200]: 47.5 vs 61.0%), whereas obtaining slightly higher cell alignment efficiency on PUX$_{HP}$-PCL[x500y200] ([x500y200] vs [x200y200]: 68.8 vs 61.0%). MSCs cultured on PUX$_{HP}$-PCL[x500y200] showed a considerable increase in the cell alignment efficiency as compared to that of PUX$_{HP}$-PCL[x200y500] (21.3% increase, p < 0.001).

Substrate feature edges have been proposed as nucleation sites to facilitate cell adhesion.[32] In this study, the observations on MSCs demonstrated that cells preferentially distributed around the holes of PUX$_{HP}$-PCL (Figure 4c,d). If cells could extend freely over the holes, MSCs would still align along the ridges/grooves. If only one cell extension end was obstructed at the hole edges, MSCs would conform their shapes to the holes, and exhibited as half-cell alignment along the ridge direction. However, if one end of the cell was obstructed at the holes and the other protrusions crossed over the ridges/grooves to attach to the adjacent film surface points, MSCs would organize themselves to deviate from the ridge direction, resulting in reduced cell alignment efficiency. These explained how the presence of laser-induced holes interfered with cell alignment along the micropatterned ridges/grooves. It should be noted that as compared to PUX$_{HP}$-PCL[x200y200], more cells were found to distribute in the adjacent areas of holes for UX$_{HP}$-PCL[x200y500] (Figure 4b,c). This phenomena could be attributed to the increased interhole distance in y-axis that weakened the attraction of holes to cells.[32] Furthermore, although the interhole distance for PUX$_{HP}$-PCL[x200y200] was 200 μm in both x and y-axes (within the length of elongated MSCs: ~100−400 μm; Figure 4b), cells have been observed to anchor and bridge the two-adjacent holes in x-axis but not in y-axis, suggesting that the ridges/grooves of PUX$_{HP}$-PCL could impact MSCs organization more than the holes did.

The fact that MSCs cultured on PUX$_{HP}$-PCL with different spatial hole distributions obtained different alignment efficiencies demonstrated that the influences of laser-induced holes on MSCs alignment were dependent on the interhole distance. An interhole distance of 200 μm in x-axis would enable MSCs to bridge the two-adjacent holes, and if the cells were unable to extend over holes, they would adjust their extension to anchor to other positions, resulting in a final cell elongation deviated from the ridges. In contrast, compared to the observed mean cell length of ~245 μm, an interhole distance of 500 μm in x-axis was sufficient to allow free cell extension of MSCs without formation of hole-to-hole bridge. Furthermore, although holes might block MSCs extension at one end, the cells remained able to extend freely at the other end. These reasons explained the observed larger cell alignment efficiency for MSCs cultured on PUX$_{HP}$-PCL[x500y200] as compared to that of cells on PUX$_{HP}$-PCL[x200y200], as there was more space for the cells to grow along the ridges. However, as compared to PUX$_{HP}$-PCL[x200y200], the increased interhole distance in y-axis (for

DOI: 10.1021/acsami.5b02464
ACS Appl. Mater. Interfaces 2015, 7, 13445−13456

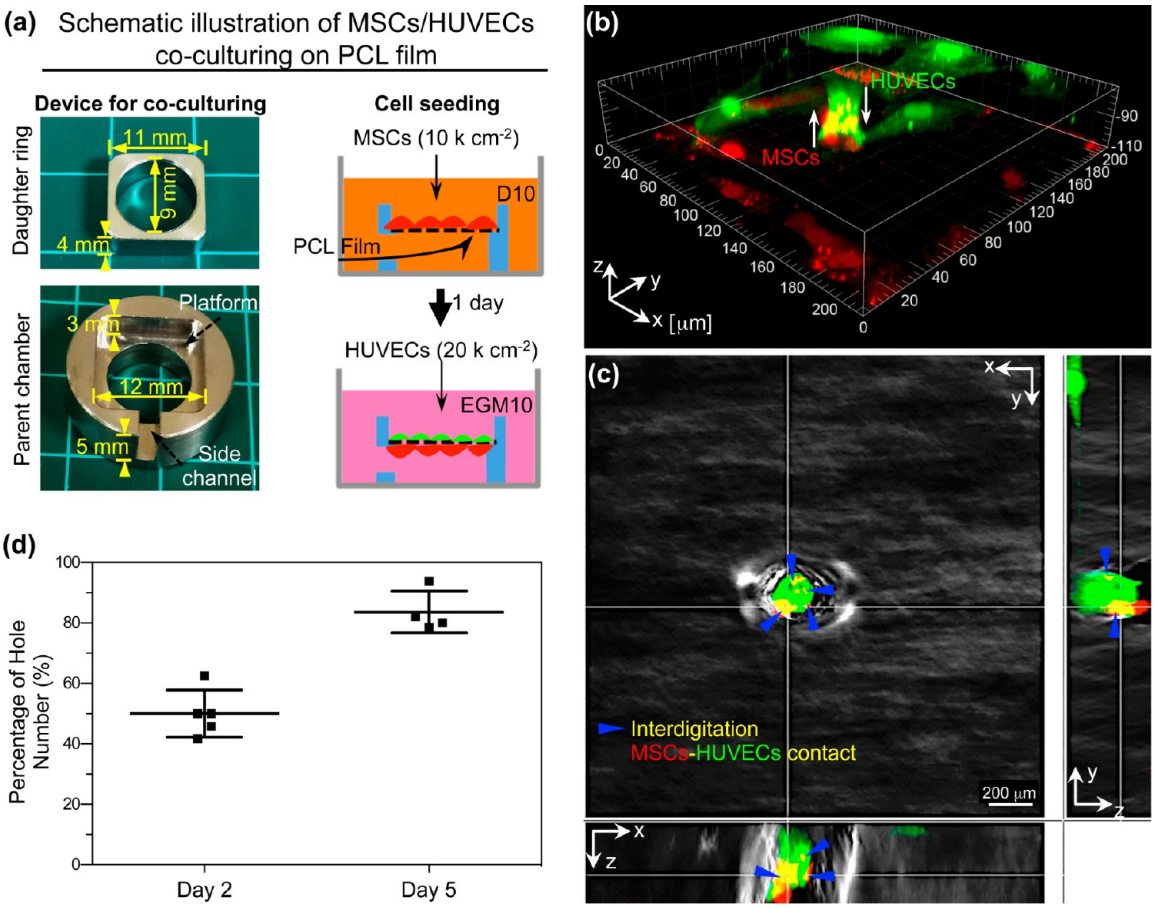

Figure 6. Transmural direct MSCs/HUVECs interaction. (a) Schematic diagrams illustrating coculture of MSCs and HUVECs on PUX_{HP}-PCL[x500y500]. PHK26-labeled MSCs (red color; 10 000 cells/cm^2) were seeded on film one surface, and after culturing in D10 medium for 1 day, GFP-labeled HUVECs (green color; 20 000 cells/cm^2) were seeded on the opposite side of the film and cocultured in EGM10 medium for 3 days. (b) 3D construction and (c) cross-sectional views of CLSM images. MSCs and HUVECs formed transmural interdigitation cell−cell contact (white arrow, cell ingrowth into the holes; yellow color, colocalization of red and green colors; blue arrow, MSCs−HUVECs contact; scale bar = 20 μm). (d) Percentage of holes that occurred with transmural cell−cell contact for 2 and 5 days of coculturing (n = 4).

example: PUX_{HP}-PCL[x200y500]) did not result in better cell alignment efficiency. This could be attributed to the clustering of cells around the holes, due to the combined effect of weaker cell attraction in y-axis as compared to that in x-axis and a small interhole distance of 200 μm in x-axis. Comparing PUX_{HP}-PCL[x500y200] and PUX_{HP}-PCL[x200y500], MSCs cultured on the latter exhibited significantly lower cell alignment efficiency, although the interhole distance of the latter was larger. These observations indicated that the influences of increase in the interhole distance in y-axis on cell alignment efficiency could be dependent on the interhole distance in x-axis.

To interrogate the speculation, we fabricated PUX_{HP}-PCL[x500y500], and investigated the cell alignment efficiency when the interhole distance in x-axis was increased and in y-axis was kept at 500 μm (Figure 5a). Through the analysis of cellular angles, Figure 5b shows that MSCs cultured on PUX_{HP}-PCL[x500y500] for 3 days achieved comparable cell alignment efficiency to that of Pos Ctrl ($p > 0.05$). To understand that whether the laser-induced holes have accounted for the-above obtained cell alignment on PUX_{HP}-PCL[x500y500], holes were also fabricated on HP-PCL at the same interhole distance of 500 μm in both x- and y-axes (PHP-PCL[x500y500]; Figure 5a). Culturing on PHP-PCL[x500y500], MSCs exhibited a low cell alignment efficiency similar to that of Neg Ctrl (the HP-PCL group; $p > 0.05$; Figure 5b), and significantly lower than that of PUX_{HP}-PCL[x500y500] (74.2% reduction, $p < 0.001$). Upon culturing for 8 days, MSCs achieved confluence and organized themselves into multilayers, which were all well aligned for both Pos Ctrl and PUX_{HP}-PCL[x500y500] (Figure 5c). Although MSCs also obtained confluence for Neg Ctrl and PHP-PCL[x500y500], the cells remained randomly organized with localized areas of cell alignment.

The elevated cell alignment efficiency observed for MSCs cultured on PUX_{HP}-PCL[x500y500] was because the equal interhole distances in x- and y-axes caused similar cell attraction, whereas the interhole distance of 500 μm was sufficient for MSCs to extend along the ridges. Comparing PUX_{HP}-PCL[x500y200] and PUX_{HP}-PCL[x500y500], the increase of interhole distance in y-axis resulted in increased alignment efficiency for MSCs, further suggesting that how the changes of interhole distance in y-axis influenced cell alignment was dependent on the interhole distance in x-axis. It was worth noting that as compared to Pos Ctrl, MSCs on PUX_{HP}-PCL[x500y500] have achieved comparable alignment efficiency, and with prolonged culturing, they could grow into aligned cell multilayers similar as that in the native tunica media of blood vessels. These results provided a method via controlling spatial hole placement to avoid the hole interferences for engineering intact cell alignment. The

DOI: 10.1021/acsami.5b02464
ACS Appl. Mater. Interfaces 2015, 7, 13445−13456

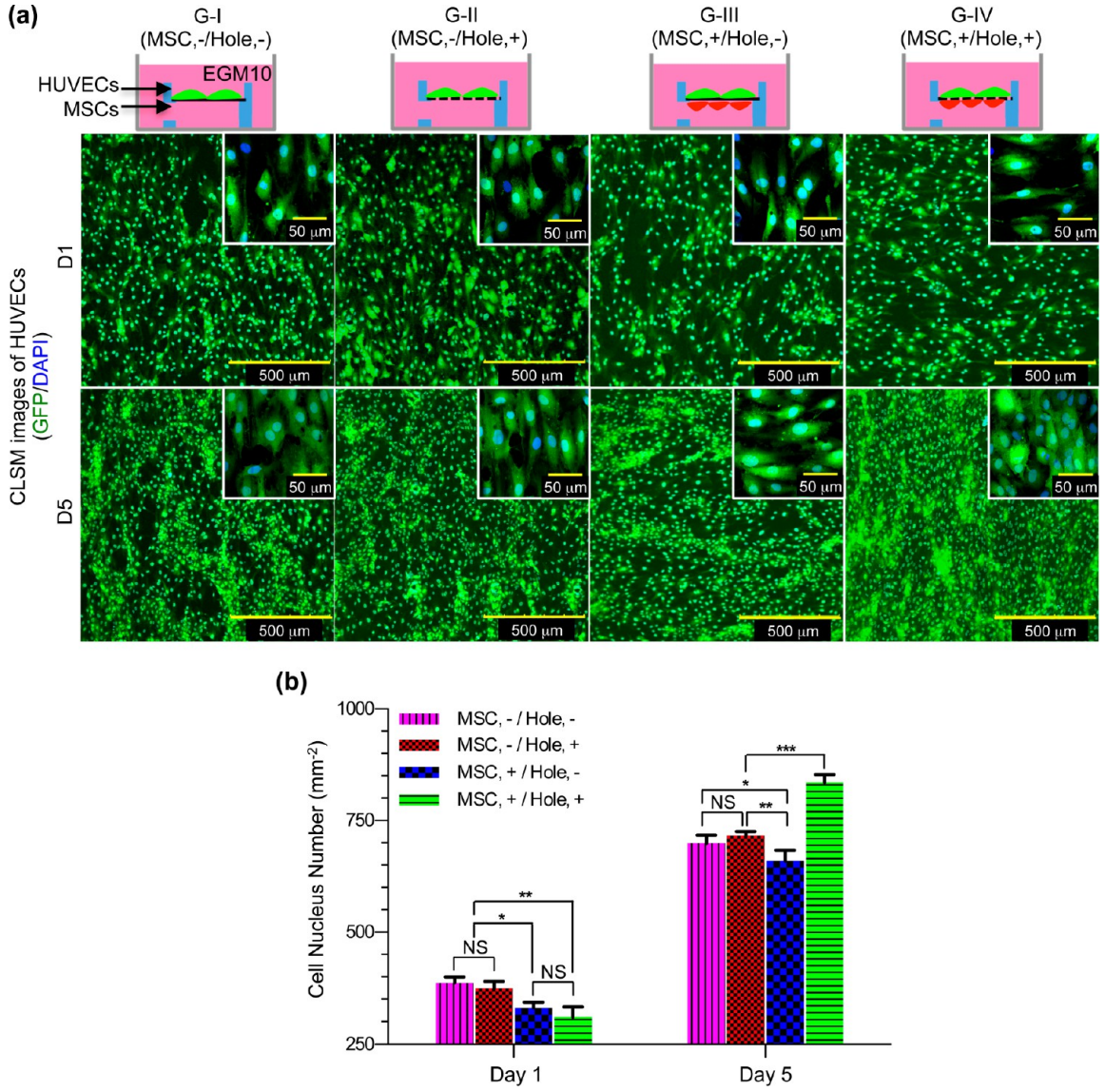

Figure 7. Cellular adhesion and proliferation of HUVECs. GFP-labeled HUVECs (green color; 20 000 cells/cm^2) were cultured on UX$_{HP}$-PCL (G-I: MSC/Hole, −/−) and PUX$_{HP}$-PCL[x500y500] (G-II: MSC/Hole, −/+) alone or cocultured with MSCs (10 000 cells/cm^2) on UX$_{HP}$-PCL (G-III: MSC/Hole, +/−) and PUX$_{HP}$-PCL[x500y500] (G-IV: MSC/Hole, +/+) in EGM10 medium for 1 and 5 days, and stained with nucleus DNA (DAPI: blue color). (a) CLSM images of HUVECs (inset: high-magnified CLSM images). (b) Quantitative analysis of nucleus numbers of HUVECs (cells labeled with GFP and nuclei). HUVECs showed increased cell proliferation for culturing on PUX$_{HP}$-PCL[x500y500] via direct MSCs/HUVECs interaction (n = 3; *, p < 0.05; **, p < 0.01; ***, p < 0.001; NS, p > 0.05).

advantages of using MSCs as tunica media cell source as compared to the isolated mature SMCs were their wide range of sources from various tissues, more expandable capability *in vitro*, antithrombogenicity and immunecompatibility for vascular TE application.[2]

Transmural Stromal/Endothelial Cell Interaction via the Through-Holes of PUX$_{HP}$-PCL. The capability of PUX$_{HP}$-PCL[x500y500] was then interrogated for coculturing stromal and endothelial cells in the context of an engineered blood vessel. As shown in Figure 6a, an in-house developed device, composed of a parent chamber and a daughter ring, was used for coculturing MSCs and HUVECs as different layers located on the two surfaces of PUX$_{HP}$-PCL. The parent chamber had a platform designed for film placement, and a side channel for the mass exchange between the inside and outside environments. The daughter ring served for locating the film as well as to facilitate top-down cell seeding. Figure 6b shows the z-stacked CLSM image of a setup with cocultured PHK26-labeled MSCs and GFP-labeled HUVECs on the film's bottom and top surfaces, respectively. PUX$_{HP}$-PCL[x500y500] allowed in-growth of MSCs and HUVECs to come into contact with each cell type within the through-holes (colocalization of the red and green colors representing as a yellow color). The cross-sectional views of z-stacked CLSM image demonstrated that MSCs and HUVECs formed transmural interdigitation contact, with yellow color observed not only at the main margin of red and green colors, but also as dots embedded within both colors (Figure 6c). These results suggested that PUX$_{HP}$-PCL could support direct MSCs/HUVECs interaction, via formation of transmural interdigitation cell−cell contact as that observed for ECs and stromal cells during embryonic differentiation.[15] Moreover, as shown in Figure 6d, the enumeration of hole number from CLSM images showed that for 2 and 5 days of

DOI: 10.1021/acsami.5b02464
ACS Appl. Mater. Interfaces 2015, 7, 13445−13456

coculturing, transmural MSCs−HUVECs contact has been observed in 50.0 and 83.7% of holes, respectively.

During the development of blood vessels, ECs accounted for the synthesis of endothelial BM.[33] This nascent endothelial BM was not entirely continuous, and possessed gaps for the SMCs[5] and pericytes[15] recruiting from the circulation to form transmural heterotypic contact with ECs. In the mature vessels, SMCs/pericytes have also been observed to physically contact with ECs via the intermittent holes across endothelial BM (0.5−1.5 μm in large vessels and 0.1−0.45 μm in small vessels).[13,14,16] Similar to SMCs and pericytes, MSCs were also mesenchymally derived, and published studies have suggested that MSCs resided in a perivascular niche and could form physical contact with ECs.[34,35] Such transmural heterotypic contact between stromal (e.g., MSCs,[34,36] SMCs[5,13,17] and pericytes)[14] and endothelial cells was important for the stabilization of new vessels against regression,[5] and have been known to act critical roles for the maintenance of normal vascular structure,[13,17,34] signaling pathways (e.g., NO)[37] and functions (e.g., MSCs[36] and SMCs[38] differentiation, and ECs proliferation).[39] Previously, different strategies such as collagen gel,[34] microcarriers[40] and direct coculture[41] have been developed for realizing direct SMCs−ECs and MSCs−ECs contact. However, these coculturing systems might be limited for the translational research in vascular tissue reconstruction, as they were incapable of either guiding stromal cell alignment into the ordered tunica media-like architecture or forming correct vessel structure with distinct tunica media/BM/intima layers. In contrast, the newly developed flexible and thin film of PUX_{HP}-PCL in this study demonstrated its capability of delivering cues for aligning stromal cell multilayers. The film has further enabled transmural heterocellular contact, whereas as an interactive interface separated MSCs and HUVECs layers into a hierarchical structure as that of the native blood vessel wall. Such transmural heterocellular contact between the engineered stromal and endothelial components could be attributed to the increased hydrophilicity on tunnel surface of the through-holes due to the effects of photothermal and photochemical ablations, which facilitated cell protrusion ingrowth and anchoring.[25,42]

Despite the recapitulated structure complexity of anisotropy and intermittent absence, it should be noted that PUX_{HP}-PCL might not mimic endothelial BM at the actual scale. In this study, the through-holes were engineered at ∼10 μm in diameter, as PUX_{HP}-PCL was thicker (∼38 μm) than actual endothelial BM (∼500 nm).[7] With the same hole height, smaller hole diameters would inhibit cellular ingrowth,[43] whereas bigger through-holes typically larger than 10 μm could result in cell loss (the diameters of MSCs and HUVECs in medium suspension: ∼15−20 μm) during the cellular seeding and culture process. Compared to the existing largest holes of actual endothelial BM, the engineered through-hole diameter of this study was off by 6.7×. However, the exclusive comparison on hole diameter was not advisible, as hole height determined the distance for cells to overcome the migrating across the film. Taken the two factors into consideration, the aspect ratio of through-hole height to diameter for PUX_{HP}-PCL was ∼3.8 within the range of the actual endothelial BM (∼0.3−5),[13,16] suggesting that the engineered through-holes of PUX_{HP}-PCL could be physiologically relevant. It should also been noted that the occurrence of transmural cell−cell contact *in vivo* relied on the intermittent holes of endothelial BM. However, in physiological conditions, transmural cell−cell contact occurred in the intermittent holes of endothelial BM was not a few, depending on the types of blood vessels with a reported probability up to ∼57.5%,[44] and signals for important function regulation (e.g., cell differentiation) could be fast transmitted to adjacent cells in a wide range, probably through the cell−cell gap junctions.[37,38,45] Therefore, it was not indispensable for all the surface-areas of endothelial BM and PUX_{HP}-PCL to have the holes.

Rapid Endothelialization on PUX_{HP}-PCL Surface. To reconstruct tunica intima, HUVECs were cocultured on the opposite side of the film, and the influences of transmural heterocellular contact on PUX_{HP}-PCL's endothelialization were assessed. Figure 7a shows the four investigated groups: single-culturing of HUVECs alone on UX_{HP}-PCL (G-I: MSC/Hole, −/−) and PUX_{HP}-PCL[x500y500] (G-II: MSC/Hole, −/+), and coculturing of HUVECs and MSCs using UX_{HP}-PCL (G-III: MSC/Hole, +/−) and PUX_{HP}-PCL[x500y500] (G-IV: MSC/Hole, +/+). CLSM images show that with 1 day of culturing, HUVECs were able to adhere on the PCL film surfaces of all four groups, with spread and elongated cellular shapes. These cells proliferated for the prolonged culturing for 5 days, and appeared to spread out in a typical cobblestone-like morphology similar to the ECs morphology *in vivo*.[46] Furthermore, in all the investigated groups, HUVECs exhibited typically layered-growth, without formation of the tubular-like networks as previously reported when ECs were coexisted with myogenic-related cells (e.g., MSCs[19] and fibroblast)[47] without barrier separation. Such observation indicated that the transmural migration of MSCs across PUX_{HP}-PCL was inhibited. It has been suggested that for transmural stromal cell migration, the intermittent holes of endothelial BM (∼500 nm in thickness) should be greater than 3−4 μm.[44] Comparatively, the through-hole diameter in this study was ∼10 μm, but the through-hole height (∼38 μm) was 75× over that of the actual endothelial BM. Therefore, our result suggested that besides hole diameter, hole height also influenced whether the cells could migrate successfully across the film. On the other hand, MSCs were antithrombogenic, and would not induce platelet adhesion or thrombus formation even if they were presented on the endothelium side.[48,49]

Cellular nucleus counting showed that for 1 day of culturing, HUVECs in G-II exhibited a comparable nucleus number to that of the cells in G-I ($p > 0.05$), suggesting that laser-perforated through-holes have not altered the cellular adhesion of HUVECs on PCL films. However, as compared to the single-culturing of HUVECs in G-I and II, coculturing with MSCs in G-III and IV for 1 day resulted in reduced HUVECs adhesion on PCL film surfaces (Figure 7b). This lowered ECs adhesion in the presence of MSCs has previously also been shown in the direct coculturing of ECs with MSCs.[50] With the prolonged culturing for 5 days, HUVECs exhibited the similar cellular proliferation in G-I and II ($p > 0.05$). Such observation agreed with the previous report that holes with dimensions on the order of several micrometers could not affect cellular proliferation as compared to the cells on nonhole surfaces.[32] However, the prolonged culturing resulted in considerable increase in the cell proliferation of HUVECs in G-IV, which was higher than those of both the single-culturing in G-I and II (16.7−19.6% increase, $p < 0.001$) and the coculturing in G-III (26.8% increase, $p < 0.001$) groups. Comparatively, coculturing of MSCs and HUVECs using UX_{HP}-PCL allowed paracrine secretion for indirect MSCs/HUVECs interaction, whereas coculturing using PUX_{HP}-PCL could enable both indirect and

DOI: 10.1021/acsami.5b02464
ACS Appl. Mater. Interfaces 2015, 7, 13445−13456

direct MSCs/HUVECs interactions via paracrine secretion and transmural cell−cell contact, respectively. The increased proliferation of HUVECs in G-IV could be attributed to the transmural MSCs−HUVECs contact, which has been known with stabilized effects on nascent endothelium to avoid regression.[5,34,39] Consistently with this, HUVECs cocultured with indirect MSCs/HUVECs interaction in G-III for 5 days remained with a lower number of cell nuclei as compared to that of HUVECs single-culturing groups (vs G-I, 6.0% reduction, $p < 0.05$; vs G-II, 8.0% reduction, $p < 0.001$).

Bioactivity of PUX_{HP}-PCL-based Vascular Construction. The bioactivity of coculturing-resulted MSCs/PCL/HUVECs construct was evaluated by measuring the total level of system NO, which has been known as an important inhibitor for preventing platelet aggregation and leukocyte adhesion.[51,52] Figure 8 shows total NO levels of different

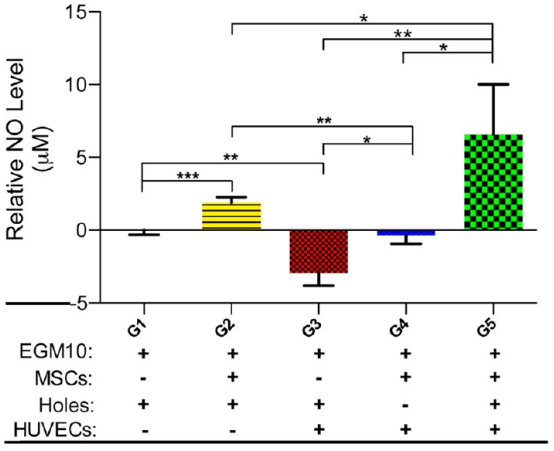

Figure 8. Total NO levels for vascular tissue construction systems. MSCs (10 000 cells/cm^2) and HUVECs (20 000 cells/cm^2) were cultured in EGM10 for 8 days. Total NO level was measured for EGM10 medium alone (G1), single-culturing of MSCs (G2) and HUVECs (G3) on PUX_{HP}-PCL[x500y500], coculturing of MSCs/HUVECs on UX_{HP}-PCL (G4), and coculturing of MSCs/HUVECs on PUX_{HP}-PCL[x500y500] (G5). Vascular tissue construction based on PUX_{HP}-PCL[x500y500] with direct MSCs/HUVECs interaction resulted in an elevated total NO level ($n = 3$; *, $p < 0.05$; **, $p < 0.01$; ***, $p < 0.001$).

vascular tissue construction systems after 8 days of culturing. Compared to the culturing medium of EGM10 (G1), single-culturing of MSCs (G2) resulted in an increased total NO level ($p < 0.001$), whereas a reduced total NO level was observed for single-culturing of HUVECs (G3, $p < 0.01$). Such declined total NO level agreed with the observations of previously published studies, which demonstrated that ECs could consume NO.[53,54] One possible mechanism behind the observed NO consumption could be attributed to an intracellular dioxygenase via direct oxidation.[53,54] Furthermore, in recent studies, human ECs were reported to express hemoglobin (an iron [Fe^{2+}/Fe^{3+}]-containing metalloprotein well-known for NO metabolism), which could also contribute to the observed endothelial NO consumption.[55−57] Previously, there were some studies showing higher total NO levels when the medium was cultured with ECs.[58,59] These studies, however, were not contradictory to the results in this study, as the cellular culture periods for NO detection were distinct (less than 2 days for those studies, and 8 days of cell culturing in this study), which could affect significantly the measured total NO levels.[60]

Further increase in total NO level has been observed for coculturing via PUX_{HP}-PCL[x500y500] (vs G2:2.5× increase, $p < 0.05$). In contrast, coculturing of MSCs and HUVECs using UX_{HP}-PCL remained a lower total NO level than that of either MSCs single-culturing or coculturing via PUX_{HP}-PCL-[x500y500] ($p < 0.01$). These results showed that transmural MSCs−HUVECs contact resulted in an elevated total NO level for the vascular tissue construction system. This obtained total NO level could be released from both MSCs[61] and HUVECs,[51] and was in a comparable order to that of the cocultured quiescent SMCs and ECs.[51] These observations suggested that PUX_{HP}-PCL with incorporation of MSCs and HUVECs could be promising for applications in vascular tissue engineering.

CONCLUSIONS

Herein, we developed a novel bioresponsive film with dual-microstructured geometries, for biomimicking the architectural roles of the endothelial BM in developing vessels. Flexible PCL thin film obtained microscale anisotropic ridges/grooves and through-holes via a combination of uniaxial thermal stretching and direct laser perforation processes. Human MSCs cultured on the PCL film tended to exhibit aligned organization along the ridges/grooves, whereas in the presence of holes, these cells showed disturbed organization deviating from the ridge direction. Through optimizing the interhole distance, MSCs obtained an intact cell alignment efficiency on the PCL film. With prolonged culturing for 8 days, these cells formed aligned cell multilayers as found in the native tunica media. Coculturing on the opposite side of the film, HUVECs exhibited direct interaction with MSCs via formation of transmural interdigitation cell−cell contact, leading to a rapid endothelialization on the PCL film surface. Such a coculturing-resulted MSC/PCL/HUVEC construct showed enhanced bioactivity with an elevated total NO level, as compared to the single MSCs or HUVECs culturing and indirect MSCs/HUVECs coculturing systems. These results provide insights to how the structural biomimicking of endothelial BM regulates vascular cell responses. The dual-microstructured porous and anisotropic film could be used as an engineered endothelial BM for vascular tissue reconstruction.

AUTHOR INFORMATION

Corresponding Authors

*E. S. Thian. E-mail: mpetes@nus.edu.sg. Tel: (65) 6516 5233. Fax: (65) 6779 1459.

*J. K. Y. Chan. E-mail: jerry.chan.ky@kkh.com.sg. Tel: (65) 6394 1051. Fax: (65) 6394 1618.

Author Contributions

The paper was written through contributions of all authors. All authors have given approval to the final version of the paper.

Notes

The authors declare no competing financial interest.

ACKNOWLEDGMENTS

The authors thank Dr. Mark Seow Khoon Chong from Nanyang Technological University and Mr. Sandikin Dedy from National University of Singapore for their assistance in cell isolation and labeling, and Dr. Qinyuan Zhang from National University of Singapore for the assistance in NO detection in this project. This work was supported by grant from the Ministry of Education, Singapore (R 265-000-300-112). Dr. Jerry Chan received salary support from the Ministry

DOI: 10.1021/acsami.5b02464
ACS Appl. Mater. Interfaces 2015, 7, 13445−13456

of Health's (Singapore) NMRC Clinician-Scientist Award (NMRC/CSA/043/2012).

REFERENCES

(1) Cardiovascular Diseases (CVDs). World Health Organization Fact Sheet [online], January, 2015. http://www.who.int/mediacentre/factsheets/fs317/en/ (accessed February 01, 2015).
(2) Wang, Z.; Teoh, S. H.; Johana, N. B.; Chong, M. S.; Teo, E. Y.; Hong, M.; Chan, J. K.; Thian, E. S. Enhancing Mesenchymal Stem Cell Response Using Uniaxially Stretched Poly(ε-caprolactone) Film Micropatterns for Vascular Tissue Engineering Application. *J. Mater. Chem. B* **2014**, *2*, 5898−5909.
(3) Liu, Y.; Lu, J.; Li, H.; Wei, J.; Li, X. Engineering Blood Vessels through Micropatterned Co-culture of Vascular Endothelial and Smooth Muscle Cells on Bilayered Electrospun Fibrous Mats with pDNA Inoculation. *Acta Biomater.* **2015**, *11*, 114−125.
(4) Gong, Z. D.; Niklason, L. E. Small-Diameter Human Vessel Wall Engineered from Bone Marrow-Derived Mesenchymal Stem Cells (hMSCs). *FASEB J.* **2008**, *22*, 1635−1648.
(5) Scheppke, L.; Murphy, E. A.; Zarpellon, A.; Hofmann, J. J.; Merkulova, A.; Shields, D. J.; Weis, S. M.; Byzova, T. V.; Ruggeri, Z. M.; Iruela-Arispe, M. L. Notch Promotes Vascular Maturation by Inducing Integrin-Mediated Smooth Muscle Cell Adhesion to the Endothelial Basement Membrane. *Blood* **2012**, *119*, 2149−2158.
(6) Eble, J. A.; Niland, S. The Extracellular Matrix of Blood Vessels. *Curr. Pharm. Des.* **2009**, *15*, 1385−1400.
(7) Liliensiek, S. J.; Nealey, P.; Murphy, C. J. Characterization of Endothelial Basement Membrane Nanotopography in *Rhesus macaque* as a Guide for Vessel Tissue Engineering. *Tissue Eng., Part A* **2009**, *15*, 2643−2651.
(8) Dickinson, L. E.; Rand, D. R.; Tsao, J.; Eberle, W.; Gerecht, S. Endothelial Cell Responses to Micropillar Substrates of Varying Dimensions and Stiffness. *J. Biomed. Mater. Res., Part A* **2012**, *100*, 1457−1466.
(9) Zorlutuna, P.; Rong, Z.; Vadgama, P.; Hasirci, V. Influence of Nanopatterns on Endothelial Cell Adhesion: Enhanced Cell Retention under Shear Stress. *Acta Biomater.* **2009**, *5*, 2451−2459.
(10) Gasiorowski, J. Z.; Liliensiek, S. J.; Russell, P.; Stephan, D. A.; Nealey, P. F.; Murphy, C. J. Alterations in Gene Expression of Human Vascular Endothelial Cells Associated with Nanotopographic Cues. *Biomaterials* **2010**, *31*, 8882−8888.
(11) Melchiorri, A. J.; Hibino, N.; Fisher, J. P. Strategies and Techniques to Enhance the In Situ Endothelialization of Small-Diameter Biodegradable Polymeric Vascular Grafts. *Tissue Eng., Part B* **2013**, *19*, 292−307.
(12) Park, J.; Bauer, S.; Schmuki, P.; von der Mark, K. Narrow Window in Nanoscale Dependent Activation of Endothelial Cell Growth and Differentiation on TiO_2 Nanotube Surfaces. *Nano Lett.* **2009**, *9*, 3157−3164.
(13) Sandow, S. L.; Senadheera, S.; Bertrand, P. P.; Murphy, T. V.; Tare, M. Myoendothelial Contacts, Gap Junctions, and Microdomains: Anatomical Links to Function? *Microcirculation* **2012**, *19*, 403−415.
(14) Armulik, A.; Abramsson, A.; Betsholtz, C. Endothelial/Pericyte Interactions. *Circ. Res.* **2005**, *97*, 512−523.
(15) Bou-Gharios, G.; Ponticos, M.; Rajkumar, V.; Abraham, D. Extra-Cellular Matrix in Vascular Networks. *Cell Proliferation* **2004**, *37*, 207−220.
(16) Saunders, K. B.; D'Amore, P. A. An in Vitro Model for Cell-Cell Interactions. *In Vitro Cell. Dev. Biol.* **1992**, *28A*, 521−528.
(17) Heydarkhan-Hagvall, S.; Helenius, G.; Johansson, B. R.; Li, J. Y.; Mattsson, E.; Risberg, B. Co-culture of Endothelial Cells and Smooth Muscle Cells Affects Gene Expression of Angiogenic Factors. *J. Cell. Biochem.* **2003**, *89*, 1250−1259.
(18) Wang, Z.; Teo, E. Y.; Chong, M. S.; Zhang, Q.; Lim, J.; Zhang, Z.; Hong, M.; Thian, E. S.; Chan, J. K.; Teoh, S. H. Biomimetic Three-Dimensional Anisotropic Geometries by Uniaxial Stretch of Poly(ε-caprolactone) Films for Mesenchymal Stem Cell Proliferation, Alignment, and Myogenic Differentiation. *Tissue Eng., Part C* **2013**, *19*, 538−549.
(19) Liu, Y.; Teoh, S. H.; Chong, M. S.; Lee, E. S.; Mattar, C. N.; Randhawa, N. S. K.; Zhang, Z.; Medina, R. J.; Kamm, R. D.; Fisk, N. M. Vasculogenic and Osteogenesis-Enhancing Potential of Human Umbilical Cord Blood Endothelial Colony-Forming Cells. *Stem Cells* **2012**, *30*, 1911−1924.
(20) Wang, Z.; Lim, J.; Ho, Y. S.; Zhang, Q.; Chong, M. S.; Tang, M.; Hong, M.; Chan, J. K.; Teoh, S. H.; Thian, E. S. Biomimetic Three-Dimensional Anisotropic Geometries by Uniaxial Stretching of Poly(ε-caprolactone) Films: Degradation and Mesenchymal Stem Cell Responses. *J. Biomed. Mater. Res., Part A* **2014**, *102*, 2197−2207.
(21) Lee, M.; Wu, B. M.; Dunn, J. C. Effect of Scaffold Architecture and Pore Size on Smooth Muscle Cell Growth. *J. Biomed. Mater. Res., Part A* **2008**, *87*, 1010−1016.
(22) Woodruff, M. A.; Hutmacher, D. W. The Return of a Forgotten Polymer-Polycaprolactone in The 21st Century. *Prog. Polym. Sci.* **2010**, *35*, 1217−1256.
(23) Sugioka, K.; Cheng, Y. Ultrafast Lasers-Reliable Tools for Advanced Materials Processing. *Light: Sci. Appl.* **2014**, *3*, e149.
(24) Aguilar, C. A.; Lu, Y.; Mao, S.; Chen, S. Direct Micro-Patterning of Biodegradable Polymers Using Ultraviolet and Femtosecond Lasers. *Biomaterials* **2005**, *26*, 7642−7649.
(25) Klein, R. *Laser Welding of Plastics*; Wiley-VCH Verlag GmbH: Weinheim, Germany, 2012.
(26) Li, H.; Xu, Y.; Xu, H.; Chang, J. Electrospun Membranes: Control of The Structure and Structure Related Applications in Tissue Regeneration and Drug Delivery. *J. Mater. Chem. B* **2014**, *2*, 5492−5510.
(27) Gaharwar, A. K.; Nikkhah, M.; Sant, S.; Khademhosseini, A. Anisotropic Poly(glycerol sebacate)-Poly(ε-caprolactone) Electrospun Fibers Promote Endothelial Cell Guidance. *Biofabrication* **2015**, *7*, 015001.
(28) Baker, B. M.; Gee, A. O.; Metter, R. B.; Nathan, A. S.; Marklein, R. A.; Burdick, J. A.; Mauck, R. L. The Potential to Improve Cell Infiltration in Composite Fiber-Aligned Electrospun Scaffolds by The Selective Removal of Sacrificial Fibers. *Biomaterials* **2008**, *29*, 2348−2358.
(29) Miller, D. C.; Thapa, A.; Haberstroh, K. M.; Webster, T. J. Endothelial and Vascular Smooth Muscle Cell Function on Poly-(lactic-co-glycolic acid) with Nano-Structured Surface Features. *Biomaterials* **2004**, *25*, 53−61.
(30) Lu, J.; Rao, M. P.; MacDonald, N. C.; Khang, D.; Webster, T. J. Improved Endothelial Cell Adhesion and Proliferation on Patterned Titanium Surfaces with Rationally Designed, Micrometer to Nanometer Features. *Acta Biomater.* **2008**, *4*, 192−201.
(31) Liliensiek, S. J.; Wood, J. A.; Yong, J.; Auerbach, R.; Nealey, P. F.; Murphy, C. J. Modulation of Human Vascular Endothelial Cell Behaviors by Nanotopographic Cues. *Biomaterials* **2010**, *31*, 5418−5426.
(32) Karuri, N. W.; Porri, T. J.; Albrecht, R. M.; Murphy, C. J.; Nealey, P. F. Nano and Microscale Holes Modulate Cell-Substrate Adhesion, Cytoskeletal Organization, and Integrin Localization in Sv40 Human Corneal Epithelial Cells. *IEEE Trans. Nanobiosci.* **2006**, *5*, 273−280.
(33) Davis, G. E.; Senger, D. R. Endothelial Extracellular Matrix: Biosynthesis, Remodeling, and Functions During Vascular Morphogenesis and Neovessel Stabilization. *Circ. Res.* **2005**, *97*, 1093−1107.
(34) Au, P.; Tam, J.; Fukumura, D.; Jain, R. K. Bone Marrow-Derived Mesenchymal Stem Cells Facilitate Engineering of Long-Lasting Functional Vasculature. *Blood* **2008**, *111*, 4551−4558.
(35) Saleh, F. A.; Whyte, M.; Genever, P. G. Effects of Endothelial Cells on Human Mesenchymal Stem Cell Activity in a Three-Dimensional in Vitro Model. *Eur. Cells Mater.* **2011**, *22*, 242−257.
(36) Lin, C. H.; Lilly, B. Endothelial Cells Direct Mesenchymal Stem Cells toward a Smooth Muscle Cell Fate. *Stem Cells Dev.* **2014**, *23*, 2581−2590.
(37) Pogoda, K.; Füller, M.; Pohl, U.; Kameritsch, P. NO, via Its Target Cx37, Modulates Calcium Signal Propagation Selectively at Myoendothelial Gap Junctions. *Cell Commun. Signaling* **2014**, *12*, 33.

DOI: 10.1021/acsami.5b02464
ACS Appl. Mater. Interfaces 2015, 7, 13445−13456

(38) Gairhe, S.; Bauer, N. N.; Gebb, S. A.; McMurtry, I. F. Serotonin Passes through Myoendothelial Gap Junctions to Promote Pulmonary Arterial Smooth Muscle Cell Differentiation. *Am. J. Physiol.: Lung Cell. Mol. Physiol.* **2012**, *303*, L767−L777.
(39) Johansson, U.; Rasmusson, I.; Niclou, S. P.; Forslund, N.; Gustavsson, L.; Nilsson, B.; Korsgren, O.; Magnusson, P. U. Formation of Composite Endothelial Cell−Mesenchymal Stem Cell Islets a Novel Approach to Promote Islet Revascularization. *Diabetes* **2008**, *57*, 2393−2401.
(40) Korff, T.; Kimmina, S.; Martiny-Baron, G.; Augustin, H. G. Blood Vessel Maturation in a 3-Dimensional Spheroidal Coculture Model: Direct Contact with Smooth Muscle Cells Regulates Endothelial Cell Quiescence and Abrogates VEGF Responsiveness. *FASEB J.* **2001**, *15*, 447−457.
(41) Wallace, C. S.; Champion, J. C.; Truskey, G. A. Adhesion and Function of Human Endothelial Cells Co-cultured on Smooth Muscle Cells. *Ann. Biomed. Eng.* **2007**, *35*, 375−386.
(42) Slepička, P.; Michaljaničová, I.; Sajdl, P.; Fitl, P.; Švorčík, V. Surface Ablation of PLLA Induced by KrF Excimer Laser. *Appl. Surf. Sci.* **2013**, *283*, 438−444.
(43) Wang, L.; Murthy, S. K.; Fowle, W. H.; Barabino, G. A.; Carrier, R. L. Influence of Micro-Well Biomimetic Topography on Intestinal Epithelial Caco-2 Cell Phenotype. *Biomaterials* **2009**, *30*, 6825−6834.
(44) Sandow, S. L.; Gzik, D. J.; Lee, R. M. Arterial Internal Elastic Lamina Holes: Relationship to Function? *J. Anat.* **2009**, *214*, 258−266.
(45) Bazzoni, G.; Dejana, E. Endothelial Cell-to-Cell Junctions: Molecular Organization and Role in Vascular Homeostasis. *Physiol. Rev.* **2004**, *84*, 869−901.
(46) Feinberg, A. W.; Wilkerson, W. R.; Seegert, C. A.; Gibson, A. L.; Hoipkemeier-Wilson, L.; Brennan, A. B. Systematic Variation of Microtopography, Surface Chemistry and Elastic Modulus and The State Dependent Effect on Endothelial Cell Alignment. *J. Biomed. Mater. Res., Part A* **2008**, *86a*, 522−534.
(47) Takahashi, H.; Shimizu, T.; Nakayama, M.; Yamato, M.; Okano, T. Anisotropic Cellular Network Formation in Engineered Muscle Tissue through the Self-Organization of Neurons and Endothelial Cells. *Adv. Healthcare Mater.* **2014**, *4*, 356−360.
(48) Hashi, C. K.; Zhu, Y.; Yang, G. Y.; Young, W. L.; Hsiao, B. S.; Wang, K.; Chu, B.; Li, S. Antithrombogenic Property of Bone Marrow Mesenchymal Stem Cells in Nanofibrous Vascular Grafts. *Proc. Natl. Acad. Sci. U. S. A.* **2007**, *104*, 11915−11920.
(49) Hashi, C. K.; Derugin, N.; Janairo, R. R. R.; Lee, R.; Schultz, D.; Lotz, J.; Li, S. Antithrombogenic Modification of Small-Diameter Microfibrous Vascular Grafts. *Arterioscler., Thromb., Vasc. Biol.* **2010**, *30*, 1621−1627.
(50) Menge, T.; Gerber, M.; Wataha, K.; Reid, W.; Guha, S.; Cox, C. S., Jr.; Dash, P.; Reitz, M. S., Jr; Khakoo, A. Y.; Pati, S. Human Mesenchymal Stem Cells Inhibit Endothelial Proliferation and Angiogenesis via Cell−Cell Contact Through Modulation of The VE-Cadherin/β-Catenin Signaling Pathway. *Stem Cells Dev.* **2012**, *22*, 148−157.
(51) Li, J.; Li, G.; Zhang, K.; Liao, Y.; Yang, P.; Maitz, M. F.; Huang, N. Co-culture of Vascular Endothelial Cells and Smooth Muscle Cells by Hyaluronic Acid Micro-Pattern on Titanium Surface. *Appl. Surf. Sci.* **2013**, *273*, 24−31.
(52) Seabra, A. B.; Justo, G. Z.; Haddad, P. S. State of The Art, Challenges and Perspectives in The Design of Nitric Oxide-Releasing Polymeric Nanomaterials for Biomedical Applications. *Biotechnol. Adv.* **2015**, DOI: 10.1016/j.biotechadv.2015.01.005.
(53) Schmidt, K.; Mayer, B. Consumption of Nitric Oxide by Endothelial Cells: Evidence for The Involvement of A NAD(P)H-, Flavin- and Heme-Dependent Dioxygenase Reaction. *FEBS Lett.* **2004**, *577*, 199−204.
(54) Gardner, P. R.; Martin, L. A.; Hall, D.; Gardner, A. M. Dioxygen-Dependent Metabolism of Nitric Oxide in Mammalian Cells. *Free Radical Biol. Med.* **2001**, *31*, 191−204.
(55) Straub, A. C.; Lohman, A. W.; Billaud, M.; Johnstone, S. R.; Dwyer, S. T.; Lee, M. Y.; Bortz, P. S.; Best, A. K.; Columbus, L.; Gaston, B. Endothelial Cell Expression of Haemoglobin α Regulates Nitric Oxide Signalling. *Nature* **2012**, *491*, 473−477.
(56) Butcher, J. T.; Johnson, T.; Beers, J.; Columbus, L.; Isakson, B. E. Hemoglobin Alpha in the Blood Vessel Wall. *Free Radical Biol. Med.* **2014**, *73*, 136−142.
(57) Gardner, P. R. Hemoglobin: A Nitric-Oxide Dioxygenase. *Scientifica* **2012**, *2012*, 683729.
(58) Ugusman, A.; Zakaria, Z.; Chua, K. H.; Nordin, N. A. M. M.; Mahdy, Z. A. Role of Rutin on Nitric Oxide Synthesis in Human Umbilical Vein Endothelial Cells. *Sci. World J.* **2014**, *2014*, 169370.
(59) Cho, H. Y.; Park, C. M.; Kim, M. J.; Chinzorig, R.; Cho, C. W.; Song, Y. S. Comparative Effect of Genistein and Daidzein on the Expression of MCP-1, eNOS, and Cell Adhesion Molecules in TNF-α-Stimulated HUVECs. *Nutr. Res. Pract.* **2011**, *5*, 381−388.
(60) Cristina de Assis, M.; Cristina Plotkowski, M.; Fierro, I. M.; Barja-Fidalgo, C.; de Freitas, M. S. Expression of Inducible Nitric Oxide Synthase in Human Umbilical Vein Endothelial Cells during Primary Culture. *Nitric Oxide* **2002**, *7*, 254−261.
(61) Bassaneze, V.; Barauna, V. G.; Lavini-Ramos, C.; Kalil, J.; Schettert, I. T.; Miyakawa, A. A.; Krieger, J. E. Shear Stress Induces Nitric Oxide-Mediated Vascular Endothelial Growth Factor Production in Human Adipose Tissue Mesenchymal Stem Cells. *Stem Cells Dev.* **2010**, *19*, 371−378.

DOI: 10.1021/acsami.5b02464
ACS Appl. Mater. Interfaces 2015, 7, 13445−13456